Artificial Intelligence Applied to Electrocardiographic Images for Scalable Screening of Transthyretin Amyloid Cardiomyopathy

Veer Sangha BS[1,2], Evangelos K Oikonomou MD, DPhil[1], Rohan Khera MD, MS[1,3,4,5]

[1]Section of Cardiovascular Medicine, Department of Internal Medicine, Yale School of Medicine, New Haven, CT, USA
[2]Department of Engineering Science, Oxford University, Oxford, UK
[3]Section of Health Informatics, Department of Biostatistics, Yale School of Public Health, New Haven, CT
[4]Section of Biomedical Informatics and Data Science, Yale School of Medicine, New Haven, CT
[5]Center for Outcomes Research and Evaluation, Yale-New Haven Hospital, New Haven, CT

Abstract Word Count: 225 words

Word Count: 2,687 words

Figures/Tables: 4 Figures / 2 Tables

Keywords: Artificial Intelligence, Electrocardiogram, Transthyretin Amyloid Cardiomyopathy, Machine Learning, Health Technology

Correspondence to:
Rohan Khera, MD, MS
195 Church Street, 6th Floor, New Haven, CT 06510
rohan.khera@yale.edu

ABSTRACT

Background: Transthyretin amyloid cardiomyopathy (ATTR-CM) remains largely under-recognized, under-diagnosed, and under-treated. We hypothesized that the myocardial remodeling of ATTR-CM may be detectable through artificial intelligence (AI) applied to 12-lead electrocardiographic (ECG) images.

Methods: Across 5 hospitals of a large U.S.-based hospital system, we identified patients with ATTR-CM, defined by the presence of a positive nuclear scan with an approved bone radiotracer or pharmacotherapy with an approved transthyretin stabilizer between 2015 and the first half of 2023. The development cohort consisted of 1,011 ECGs from 234 patients (age 79 [IQR:70-85] years, n=176 [17.4%] women), who were age- and sex-matched in a 10:1 ratio to 10,110 ECGs from 10,110 controls (age 79 [IQR:70-85] years, n=1,800 [17.7%] female). A convolutional neural network (CNN) pre-trained using a bio-contrastive pretext on ECGs before 2015 was fine-tuned for ATTR-CM using 5-fold cross-validation and subsequently tested in an independent set of cases (139 ECGs in 47 patients; age 80 [75-86] years, n=44 (31.7% women)) and matched controls (1390 ECGs and patients) from the second half of 2023.

Results: The AUROC (area under the receiver operating characteristic curve) of the AI-ECG model for discriminating ATTR-CM in the leave-out, temporally distinct dataset was 0.906 [95%CI: 0.89-0.94] (**A**), with a sensitivity of 0.85 [95%CI: 0.79-0.91] and specificity 0.80 [95%CI 0.78-0.82].

Conclusions: We demonstrate that AI applied directly to ECG images represents a promising and scalable approach for the screening of ATTR-CM.

INTRODUCTION

Transthyretin (TTR) amyloid cardiomyopathy (ATTR-CM) is a progressive and life-threatening disease, which remains largely under-recognized, under-diagnosed, and under-treated. It can be either inherited as an autosomal dominant trait secondary to mutations in the transthyretin (TTR) gene (ATTRm) or caused by abnormal deposition of wild-type transthyretin (ATTRwt).[1,2] Prior studies have reported a prevalence of 13% among patients with heart failure with preserved ejection fraction,[3] 16% among patients with severe aortic stenosis,[4] and 5% among patients with cardiac hypertrophy.[5] These individuals often undergo current standard-of-care imaging by echocardiography and often cardiac magnetic resonance imaging (CMR) but do not routinely undergo dedicated nuclear imaging to screen for cardiac amyloidosis, which would be diagnostic. Therefore, they represent populations at elevated risk who go undiagnosed. This is important as cardiac amyloidosis is associated with significant morbidity and mortality, with the estimated median survival ranging from 2 to 4 years.[6,7] In recent years, novel therapies (such as tafamidis) have emerged that can effectively modify clinical disease progression by pharmacologically inhibiting the dissociation of TTR tetramers into monomers, the crucial step that triggers the cascade of amyloid formation and deposition,[7–12] or silence its production.[13] These agents can effectively reduce the decline in functional status, quality of life, and prolong survival.[7,12,13] Given the availability of these disease-modifying therapies and their contraindication among patients with advanced heart failure (New York Heart Association class IV symptoms), there is a growing need to develop scalable tools for the timely detection of patients at risk of ATTR-CM.

It has long been known that ATTR-CM is associated with certain electrocardiographic (ECG),[14] echocardiographic, and MRI signatures,[15] which may enable the timely identification of the condition and its precursors. However, these markers lack sensitivity and specificity, contributing to the large underdiagnosis of the condition, as definitive diagnosis requires dedicated nuclear amyloid imaging.[16] However, nuclear testing by bone scintigraphy or single-photon emission computed tomography (SPECT) is resource-intensive and cannot be performed in all individuals. It is notable that the lack of

traditional diagnostics to accurately identify ATTR-CM likely represents the key reason that, even among those who undergo many of the traditional diagnostic tests, accurate and timely diagnosis of ATTR-CM remains a challenge. An ECG-powered solution for the detection of likely ATTR-CM could provide a low-cost, readily available, and standardized method of detecting ATTR-CM in populations at risk of heart failure who may not be identified in current clinical workflows.

METHODS

The Yale Institutional Review Board approved the study protocol and waived the need for informed consent as the study represents a secondary analysis of existing data. Patients who opted out of research studies at the Yale New Haven Hospital (YNHH) were excluded. An online version of the model is publicly available for research use at https://www.cards-lab.org/ecgvision-attrcm. This web application represents a prototype of the eventual application of the model, with instructions for required image standards and a version that demonstrates an automated image standardization pipeline.

Data Source and Study Population

We performed a restrospective study using 12-lead ECG signal waveform data collected during the clinical care of patients at the YNHH between 2015 and 2024. These ECGs were recorded as standard 12-lead recordings sampled at 500 Hz for 10 seconds. They were recorded on multiple different machines, with Philips PageWriter and GE MAC the most frequently used.

We reviewed the electronic health records of the Yale-New Haven Health system for patients with a diagnosis of ATTR-CM, defined as: i) presence of a positive nuclear amyloid scan with an approve bone radiotracer (i.e., 99m Tc PYP scan), or ii) pharmacological therapy with an approved transthyretin stabilizer (tafamidis [Vyndamax]). The first date of appearance for any of these conditions was labeled as the date of diagnosis, and we identified all ECGs performed within the preceding 12 months, or any time after the time of diagnosis.

Controls were defined as ECGs from patients who did not meet the criteria above and also did not have a relevant ICD code for ATTR-CM ("E85.2", "E85.82"). Controls were age-sex matched at a 1:10 ratio to confirmed cases of ATTR-CM during training and validation. To avoid data leakage across training and validation sets, splits were performed at a patient level, and we performed 5-fold cross-validation to ensure the robustness of the results. To ensure the reliability of phenotypes, all controls also had an echocardiogram performed within 15 days of the ECG during training but without a clinical diagnosis of ATTR-CM. In the cross-validation testing population, the control population was expanded to include any ECG that did not meet the criteria for having ATTR-CM and did not come from a patient with an ICD code for ATTR-CM.

Furthermore, we created an independent temporally distinct held-out test population, defined as individuals who underwent testing with a PYP scan and were diagnosed with ATTR-CM in the latter half of 2023 in YNHH. Controls were age-sex matched at a 1:10 ratio to ECGs that did not meet the criteria for having ATTR-CM and did not come from a patient with an ICD code for ATTR-CM.

Image Generation

We generated ECG images to recapitulate the variation in ECG layouts in a real-world setting. Our approach to image plotting has been previously described and represents the processing steps of ECG machines to convert acquired waveform data to printed outputs.[17,18] All ECGs were analyzed to determine whether they had 10 seconds of continuous recordings across all 12 leads. The 10-second samples were preprocessed with a one-second median filter, subtracted from the original waveform to remove baseline drift in each lead. Converting ECG signals to images was independent of model development, ensuring that the model did not learn any aspects of the processing that generated images from the signals.

ECG signals were transformed into ECG images using custom plotting software. Images were generated with a calibration of 10 mm/mV, which is standard for printed ECGs in most real-world settings. Using the Python Image Library (PIL v9.2.0), we converted all images to greyscale, then

down-sampling to 300x300 pixels regardless of their original resolution. Given that real-world ECG images may vary in the layout of leads, we created a dataset with several different plotting schemes for each signal waveform recording (**Figure 1**). Variations included but were not limited to the format of the plotted ECG, colors the original ECG was plotted in before conversion to grayscale, lead label font, size and position, and grid and signal line width. Plotted formats included the four formats used in previous studies – standard (four columns printed sequentially with each containing 2.5-second intervals from three leads as well as a rhythm strip), two-rhythm (a second rhythm lead added), alternate (two columns with simultaneous 5-second recordings in each), and shuffled (precordial leads in the first two columns and limb leads in the third and fourth). Additionally, formats with zero and three rhythm leads were plotted. Leads I, II, V1, and V5 were randomly selected as rhythm leads for images where rhythm leads were present. For evaluation, ECG images were plotted in the four formats used in previous studies. All images were rotated a random amount between -10 and 10 degrees before input into the model.

Initializing the Model

To maximize the learning of the signature of ATTR-CM from the population of patients, we utilized a novel self-supervised biometric contrastive learning approach to pretrain our deep learning model. The approach ensures label efficiency, i.e., the model is able to learn signatures of a disorder from a smaller number of labeled examples than needed for traditional deep learning. The model architecture is based on a 2-D convolutional neural network for identifying complex features in images (computer vision). In our pretraining approach, the model was first trained to identify individual patient-specific patterns in ECGs regardless of their interpretation. We have previously shown that this method improves performance on downstream tasks, especially when the label used in fine-tuning is scarce.[19] Briefly, we used 156,576 pairs of ECGs from 78,288 patients from YNHH collected between 2000 and 2015 and trained the model to identify homologies in ECG images consistent across the pairs of recordings belonging to each person. None of the ECGs on the self-supervised pre-training task represented

individuals in the eventual ATTR-CM development. Characteristics of the patients in this pre-training cohort are included in **Table 1**.

Model Architecture and Training

We built a convolutional neural network model based on the EfficientNet-B3 architecture.[20] The EfficientNet-B3 model requires images to be sampled at 300 x 300 square pixels, includes 384 layers, and has over 10 million trainable parameters. To allow label-efficient model development, we initialized the model using weights from a pretrained EfficientNet-B3 model that leveraged a novel self-supervised biometric contrastive learning approach, wherein the model was trained to identify individual patient-specific patterns in ECGs regardless of their interpretation.[19] None of the ECGs on the self-supervised pretraining task represented individuals in the model development. For training, we first unfroze the last four layers and trained the model with a learning rate of 0.01 for 2 epochs. Then, we unfroze all layers and trained the model with a learning rate of 5×10^{-6} for 6 epochs. We used an Adam optimizer, gradient clipping, and a minibatch size of 64 throughout training. The optimizer and learning rates were chosen after hyperparameter optimization. For both stages of training the model, we stopped training when validation loss did not improve in 3 consecutive epochs. A custom class-balanced loss function (weighted binary cross-entropy) based on the effective number of samples was used given that the case and control labels were not equally balanced.

Localization of Model Predictive Cues

To obtain a heatmap highlighting the portions of an ECG image that were important for predicting ATTR-CM, we used Gradient-weighted Class Activation Mapping (Grad-CAM).[21] We calculated the gradients on the final stack of filters in our EfficientNet-B3 model for each prediction. We performed a global average pooling of the gradients in each filter, emphasizing those that contributed to a prediction. We then multiplied these filters by their importance weights and combined them across filters to generate Grad-CAM heatmaps. Among the 35 positive cases with the most confident model predictions

for ATTR-CM across ECG formats (the top 25%), we averaged class activation maps across the five models to determine the most important image areas for the prediction of ATTR-CM. We took an arithmetic mean across the heatmaps and models for a given image format and overlayed this average heatmap across a representative ECG before converting the image to grayscale. Additionally, we presented individual model heatmaps for a handful of examples. The Grad-CAM intensities were converted from their original scale (0 – 1) to a color range using the jet colormap array in the Python library matplotlib, which was then overlaid on the original ECG image with an alpha of 0.3. The activation map, a 10x10 array, was upsampled to the original image size using the bilinear interpolation built into TensorFlow v2.8.0.

Statistical Analysis

Categorical variables were reported as number (percentage, %), and continuous variables as mean (standard deviation [SD]) or median (interquartile range [IQR]), as appropriate. The model's performance was presented as area under the receiver operating characteristic curve (AUROC) and area under the precision-recall curve (AUPRC). The 95% confidence intervals (CI) for AUROC and AUPRC were calculated using DeLong's algorithm and bootstrapping with 1000 iterations, respectively.[22,23] Furthermore, we reported sensitivity, specificity, positive predictive value (PPV), negative predictive value (NPV), and F1 score of the model at the model threshold for 90% sensitivity in the validation set. All statistical tests were 2-sided, and the significance level was 0.05. Analytic packages used in model development and statistical analysis are reported in **Table S1**.

RESULTS

Study Population

There were 11,781 patients with 12,650 12-lead ECGs at YNHH. The data from these patients were split into cross-validation datasets, and a temporally distinct held-out test set at a patient level, as described in the methods. Individuals in the cross-validation development population had a median age

of 79 years (IQR 70-85) at the time of ECG recording, and 1,976 (19.1%) were women. Overall, 8,674 (83.9%) were non-Hispanic White, 941 (9.1%) were non-Hispanic Black, 840 (8.1%) were Hispanic, 307 (3.0%) were from other races, and information was missing for 359 (3.5%) **(Table 1)**.

Detection of ATTR-CM

In the age- and sex-matched held-out test set comprising standard format images, the model for detecting ATTR-CM achieved an AUROC of 0.91 (**Figure 2**). A probability threshold for predicting ATTR-CM was chosen based on a sensitivity of 0.85 or higher in the validation subset. With this threshold, the model had sensitivity and specificity of 0.85 and 0.81 in the held-out test set. Overall, an ECG suggestive of ATTR-CM indicated 24-fold higher odds (OR 23.9, 95% CI, 14.7 – 38.7) of ATTR-CM (**Figure 2**). The model's performance was comparable across subgroups of age, sex, and race (**Table 2** and **Figure 2**). The model performance was also comparable across the four original layouts of ECG images in the held-out set with an AUROC of 0.91 – 0.92 for detecting ATTR-CM. Sensitivity analyses demonstrated consistent model performance on ECGs without paced rhythms, atrial fibrillation and flutter, conduction disorders, in the presence of LVH, and with and without low voltage (**Table 2**).

Localization of Predictive Cues for ATTR-CM

Class activation heatmaps of the 35 positive cases with the most confident model predictions for ATTR-CM prediction across four ECG layouts are presented in **Figure 3**. For all four formats of images, the region corresponding to leads V2 and V3 was the most important areas for the prediction of ATTR-CM. Representative images of Grad-CAM analysis in a sampled individual with positive screens showed similar patterns, with consistency across the five models developed during cross-validation (**Figure 4**).

DISCUSSION

We developed and validated an automated deep-learning model for identifying ATTR-CM from ECG images. The model was developed and tested in a diverse population and demonstrated consistent performance across patient characteristics as well as variations in ECG waveform layouts, making it ideal for screening and implementation in various settings, expanding accessibility and improving the unbiased detection of ATTR-CM. Racial and gender biases influence the detection and management of cardiovascular disease in both minority populations (black and Hispanic) and women,[24,25] contributing to disparities in the diagnosis and management of cardiac amyloidosis.[24–32] A scalable screening tool deployable to accessible images of ECGs at the point of care represents a powerful way to expand access to such populations where lack of clinical suspicion or access to advanced testing may perpetuate diagnostic disparities.

Given that racial minorities bear a higher burden of cardiovascular disease and are less likely to be diagnosed or treated, there is a unique opportunity to leverage AI and digital tools to alter the current landscape of cardiovascular care in these at-risk groups, beginning with screening for risk factors. An AI tool such as the one presented here has the potential to narrow the disparity gap in both racial minorities, as it was (1) developed in a large, racially/ethnically diverse cohort of individuals, (2) provides an unbiased detection of a highly under-diagnosed condition that seems to disproportionately affect Black participants, and (3) facilitates widespread adoption in low resource settings, which are less likely to have the infrastructure to allow for use of models applied to raw signal data.

An important observation that supports the role of this model in the early identification of disease is the excellent performance (AUROC 0.93) in younger individuals, under 65 years old. A risk-based referral that uses an AI-ECG platform combined with early intervention may decrease the risk of disease progression and subsequent adverse outcomes. Instead, early detection can add a number of quality-adjusted life years due to early detection in younger populations and the timely initiation of disease-modifying therapies.[7,12,13]

CONCLUSIONS

We developed and validated a high-performing deep learning-based model that detects ATTR-CM from images of clinical 12-lead ECGs. This approach represents an accessible strategy for the timely screening of ATTR-CM, especially in low-resource settings, with the potential to enhance care for patients.

FUNDING

The authors acknowledge support from the National Heart, Lung, And Blood Institute of the National Institutes of Health (under award numbers F32HL170592 to Dr Oikonomou, and R01HL167858 and K23HL153775 to Dr Khera), the National Institute on Aging of the National Institutes of Health (under award number R01AG089981 to Dr Khera), and the Doris Duke Charitable Foundation (under award number 2022060 to Dr Khera).

DISCLOSURE OF INTEREST

V.S. is a coinventor of 63/346,□610 and 63/484,426, and a co-founder of Ensight-AI, Inc. E.K.O. is an academic co-founder of Evidence2Health LLC, a co-inventor in patent applications (18/813,882, 17/720,068, 63/619,241, 63/177,117, 63/580,137, 63/606,203, 63/562,335, US11948230B2), has been a consultant for Caristo Diagnostics Ltd and Ensight-AI Inc, and has received royalty fees from technology licensed through the University of Oxford, outside the submitted work. R.K. is an Associate Editor of JAMA and receives research support, through Yale, from the Blavatnik Foundation, Bristol-Myers Squibb, Novo Nordisk, and BridgeBio. He is a coinventor of U.S. Provisional Patent Applications 63/177,117, 63/428,569, 63/346,610, 63/484,426, 63/508,315, 63/580,137, 63/606,203, 63/562,335, and a co-founder of Ensight-AI, Inc and Evidence2Health, LLC.

Figure 1. Examples of 9 variations in the electrocardiographic images used for convolutional neural network training.

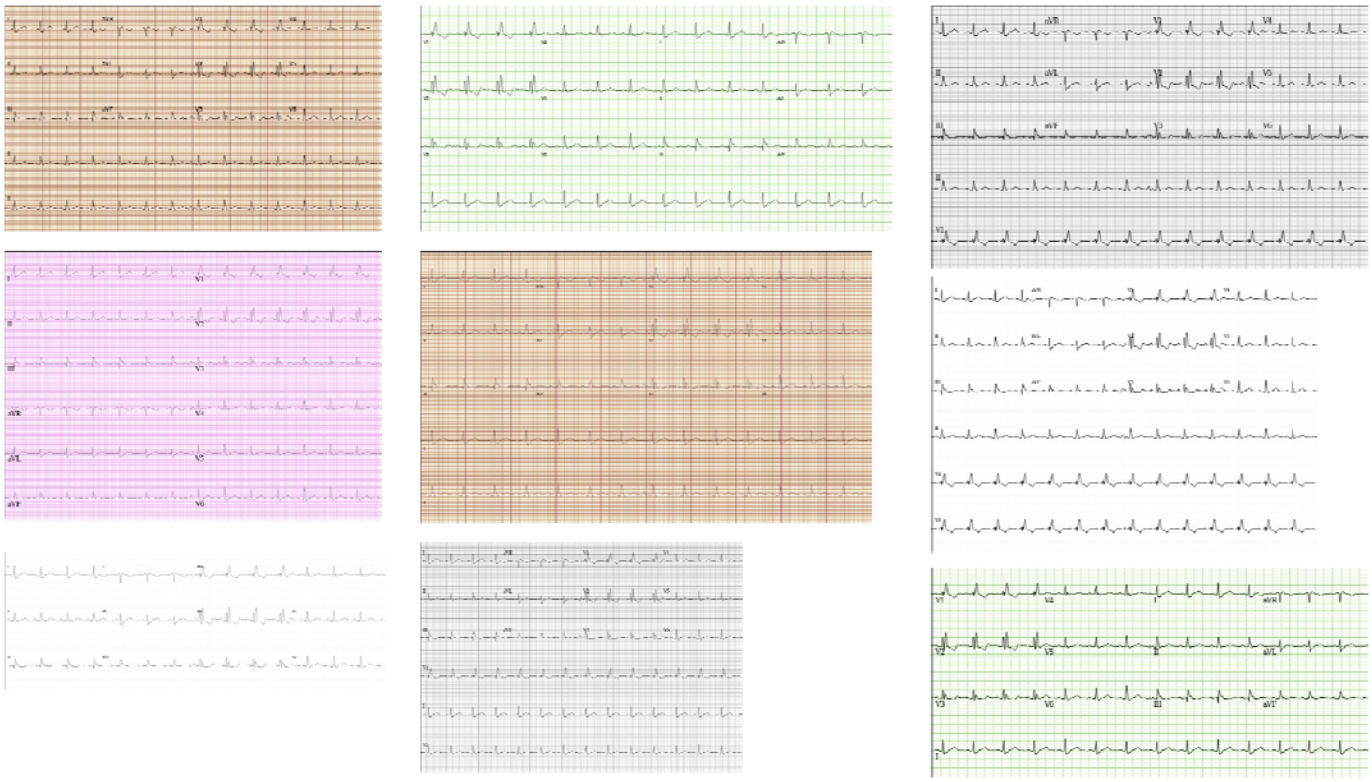

Figure 2. Model performance measures (A) Receiver operating characteristic curves across image formats in the held-out test set. B) Diagnostic odds ratios across gender, and race subgroups on standard format images in the held-out test set. Abbreviations: AUROC, area under receiver-operating characteristic curve

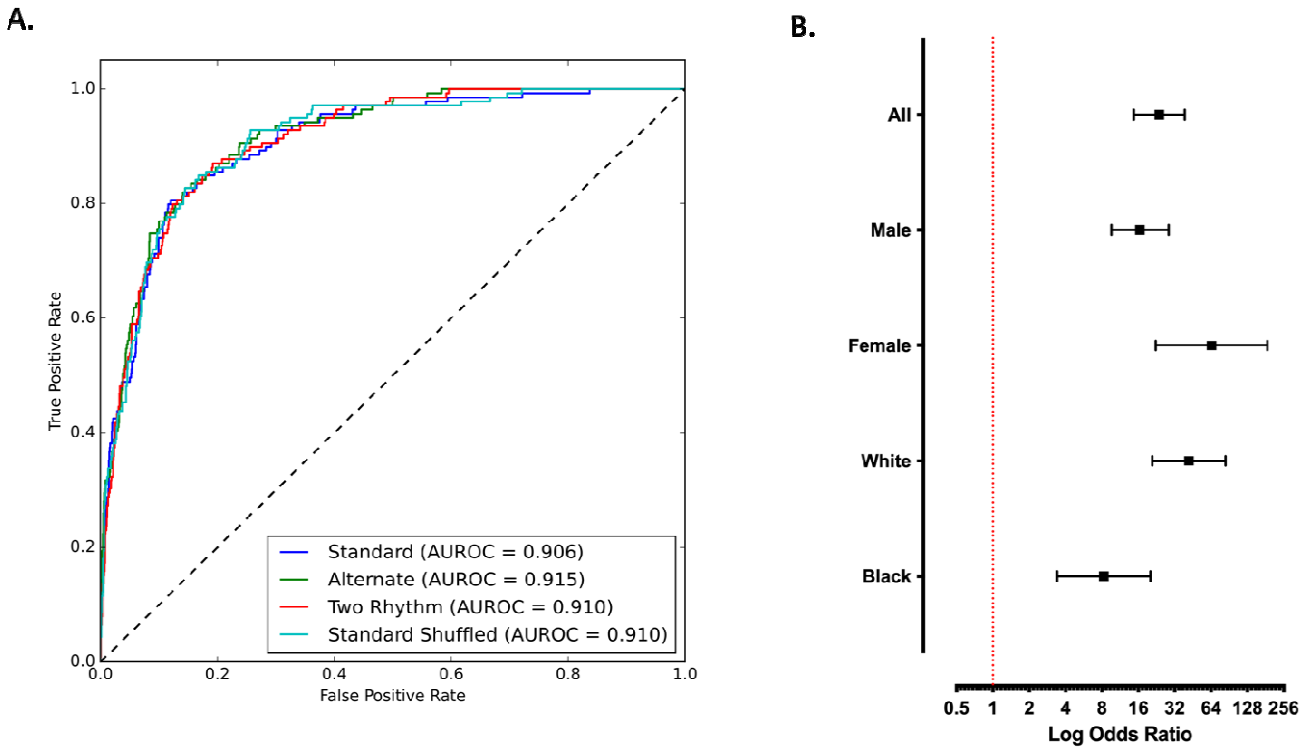

Figure 3. Gradient-weighted Class Activation Mapping (Grad-CAMs) across Electrocardiogram formats. A) Standard format B) Two rhythm leads C) Standard shuffled format D) Alternate format. The heatmaps represent averages of the 35 positive cases with the most confident model predictions for ATTR-CM.

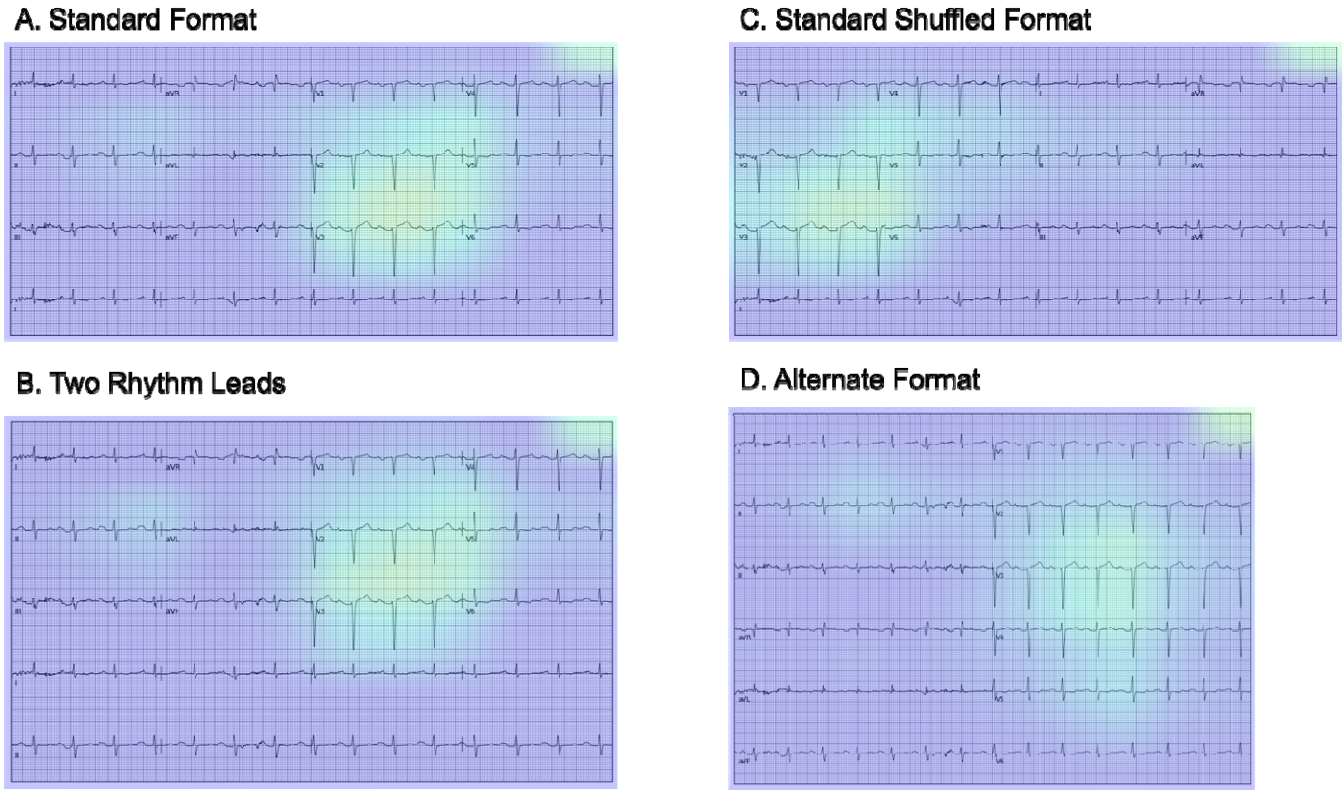

Figure 4. Gradient-weighted Class Activation Mapping (Grad-CAMs) for an example ECG with ATTR-CM. A) Average across the 5 cross validation models B) Cross Validation Model 1 C) Cross Validaiton Model 2 D) Cross Validation Model 3 E) Cross Validation Model 4 F) Cross Validation Model 5.

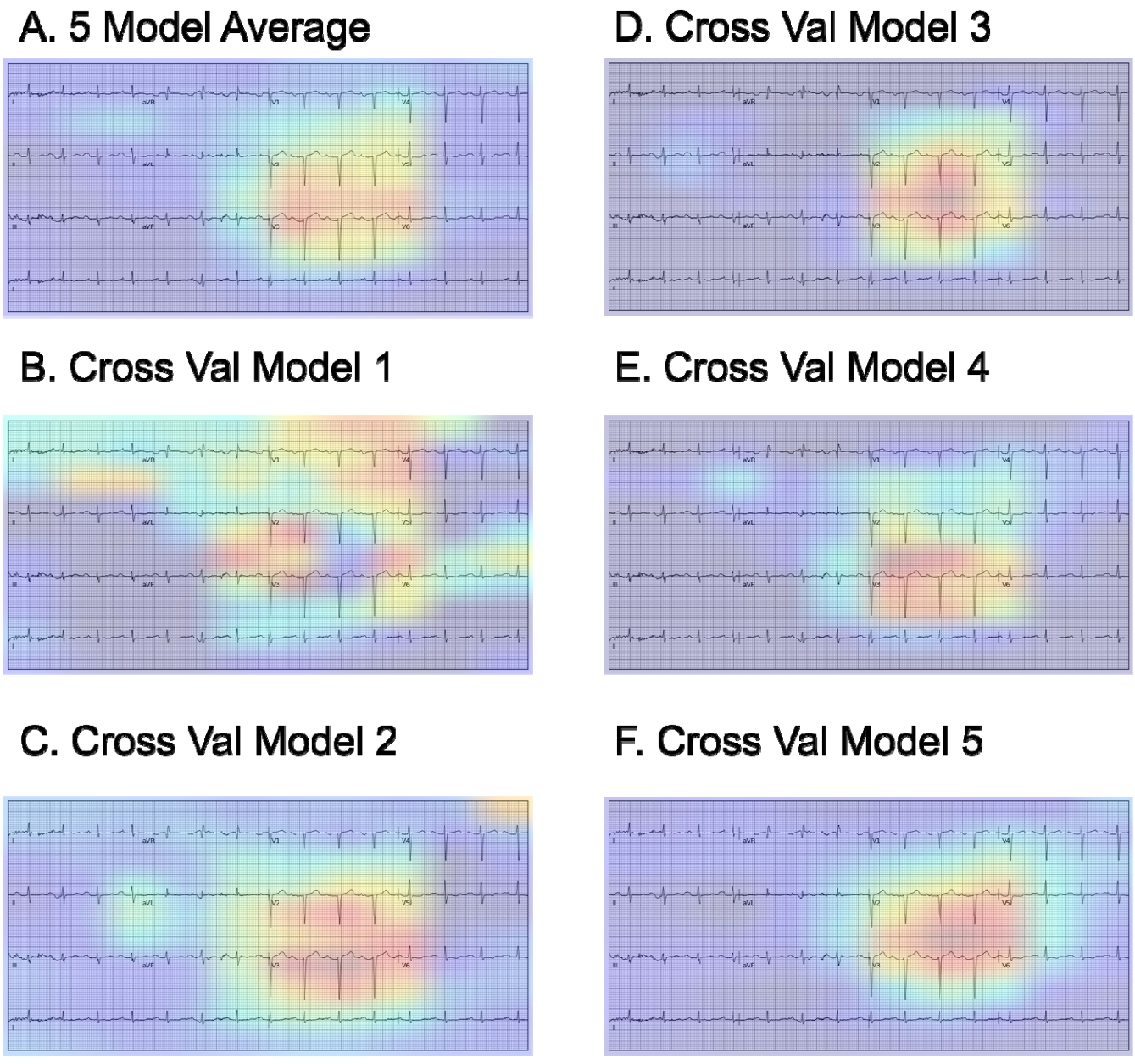

Table 1. Characteristics of Development Population. Data presented as median [IQR] for age and number (percent) for other variables. Abbreviations: ECGs, electrocardiograms; ATTR-CM, transthyretin cardiac amyloidosis.

	Pretraining	Cross Validation Development Cohort		Held-Out Test Cohort	
		ATTR-CM Cases	ATTR-CM Controls	ATTR-CM Cases	ATTR-CM Controls
Number of ECGs	156,576	1,011	10,110	139	1,390
Patients	78,288	234	10,110	47	1,390
Sex					
Female	78,784 (50.3%)	176 (17.4%)	1,800 (17.7%)	44 (31.7%)	441 (31.7%)
Male	74,146 (47.4%)	835 (82.6%)	8,310 (82.3%)	95 (68.3%)	949 (68.3%)
Missing	3,646 (2.3%)	0 (0.0%)	0 (0.0%)	0 (0.0%)	0 (0.0%)
Age (years)	60 [44 - 74]	79 [70 - 85]	79 [70 - 85]	80 [75 - 86]	80 [75 - 86]
Race					
Black	19,918 (12.7%)	176 (17.4%)	765 (7.6%)	33 (23.7%)	92 (6.6%)
Hispanic	11,464 (7.3%)	58 (5.7%)	782 (7.7%)	4 (2.9%)	72 (5.2%)
White	75,914 (48.5%)	736 (72.8%)	7,938 (78.5%)	101 (72.7%)	1140 (82.0%)
Other	2,642 (1.7%)	12 (1.2%)	295 (1.9%)	0 (0.0%)	29 (2.1%)
Unknown	46,638 (29.8%)	29 (2.9%)	330 (2.9%)	1 (0.7%)	57 (4.1%)

Table 2. Performance of model on test images across demographic subgroups in the age sex matched held-out test set.
Abbreviations: PPV, positive predictive value; NPV, negative predictive value; AUROC, area under receiver operating characteristic curve; AUPRC, area under precision recall curve; A-Fib, atrial fibrillation; ECG, electrocardiogram; LBBB, left bundle branch block; RBBB, right bundle branch block; LVH, left ventricular hypertrophy.

Labels	Number	PPV	NPV	Specificity	Sensitivity	AUROC	AUPRC	F1 Score
All	1529	0.308	0.982	0.809	0.849	0.906 (0.881-0.931)	0.562 (0.477-0.648)	0.452

Male	1044 (68.3%)	0.275	0.978	0.783	0.821	0.881 (0.845-0.917)	0.511 (0.418-0.619)	0.412
Female	485 (31.7%)	0.404	0.99	0.866	0.909	0.957 (0.937-0.978)	0.706 (0.578-0.828)	0.559
>=65	1507 (98.6%)	0.306	0.981	0.808	0.847	0.907 (0.882-0.932)	0.566 (0.477-0.65)	0.45
<65	22 (1.4%)	0.5	1	0.9	1	0.925 (0.807-1)	0.5 (0-0)	0.667
Hispanic	76 (5%)	0.25	1	0.833	1	0.951 (0.876-1)	0.546 (0-0)	0.4
White	1241 (81.2%)	0.292	0.99	0.804	0.911	0.927 (0.907-0.947)	0.534 (0.436-0.638)	0.442
Black	125 (8.2%)	0.568	0.864	0.826	0.636	0.846 (0.762-0.929)	0.751 (0.609-0.866)	0.6
Paced ECGs	109 (7.1%)	0.268	1	0.31	1	0.875 (0.807-0.943)	0.602 (0.413-0.812)	0.423
Not Paced ECGs	1420 (92.9%)	0.319	0.981	0.843	0.821	0.909 (0.882-0.937)	0.567 (0.473-0.649)	0.459
A-Fib or Flutter	280 (18.3%)	0.288	0.993	0.561	0.977	0.883 (0.832-0.934)	0.571 (0.413-0.725)	0.444
No A-Fib or Flutter	1249 (81.7%)	0.321	0.98	0.86	0.792	0.912 (0.884-0.941)	0.577 (0.467-0.676)	0.456
LBBB	79 (5.2%)	0.382	0.956	0.672	0.867	0.822 (0.701-0.943)	0.5 (0.299-0.791)	0.531
No LBBB	1413 (92.4%)	0.293	0.982	0.815	0.839	0.909 (0.882-0.936)	0.572 (0.474-0.663)	0.434
RBBB	191 (12.5%)	0.426	0.954	0.78	0.812	0.886 (0.832-0.94)	0.642 (0.478-0.784)	0.559
No RBBB	1301 (85.1%)	0.277	0.985	0.812	0.851	0.907 (0.876-0.937)	0.558 (0.465-0.656)	0.417
LVH	176 (11.5%)	0.361	0.986	0.857	0.867	0.957 (0.91-1)	0.82 (0.627-0.962)	0.51
No LVH	1353 (88.5%)	0.303	0.981	0.803	0.847	0.899 (0.872-0.927)	0.53 (0.439-0.623)	0.446
Low Voltage	108 (7.1%)	0.333	1	0.796	1	0.947 (0.904-0.99)	0.59 (0.317-0.869)	0.5
No Low Voltage	1421 (92.9%)	0.306	0.98	0.81	0.837	0.903 (0.877-0.93)	0.565 (0.48-0.649)	0.448

REFERENCES

1. Rapezzi, C. *et al.* Transthyretin-related amyloidoses and the heart: a clinical overview. *Nat. Rev. Cardiol.* **7**, 398–408 (2010).
2. Ruberg, F. L. & Berk, J. L. Transthyretin (TTR) cardiac amyloidosis. *Circulation* **126**, 1286–1300 (2012).
3. González-López, E. *et al.* Wild-type transthyretin amyloidosis as a cause of heart failure with preserved ejection fraction. *Eur. Heart J.* **36**, 2585–2594 (2015).
4. Castaño, A. *et al.* Unveiling transthyretin cardiac amyloidosis and its predictors among elderly patients with severe aortic stenosis undergoing transcatheter aortic valve replacement. *Eur. Heart J.* **38**, 2879–2887 (2017).
5. Damy, T. *et al.* Prevalence and clinical phenotype of hereditary transthyretin amyloid cardiomyopathy in patients with increased left ventricular wall thickness. *Eur. Heart J.* **37**, 1826–1834 (2016).
6. Castano, A. *et al.* Multicenter study of planar technetium 99m pyrophosphate cardiac imaging: Predicting survival for patients with ATTR cardiac amyloidosis. *JAMA Cardiol.* **1**, 880–889 (2016).
7. Maurer, M. S. *et al.* Tafamidis treatment for patients with transthyretin amyloid cardiomyopathy. *N. Engl. J. Med.* **379**, 1007–1016 (2018).
8. Fox, J. C. *et al.* First-in-human study of AG10, a novel, oral, specific, selective, and potent transthyretin stabilizer for the treatment of transthyretin amyloidosis: A phase 1 safety, tolerability, pharmacokinetic, and pharmacodynamic study in healthy adult volunteers. *Clin. Pharmacol. Drug Dev.* **9**, 115–129 (2020).
9. Nuvolone, M., Girelli, M. & Merlini, G. Oral therapy for the treatment of transthyretin-related amyloid cardiomyopathy. *Int. J. Mol. Sci.* **23**, 16145 (2022).

10. Morfino, P. *et al.* Transthyretin stabilizers and seeding inhibitors as therapies for amyloid transthyretin cardiomyopathy. *Pharmaceutics* **15**, (2023).
11. Penchala, S. C. *et al.* AG10 inhibits amyloidogenesis and cellular toxicity of the familial amyloid cardiomyopathy-associated V122I transthyretin. *Proc. Natl. Acad. Sci. U. S. A.* **110**, 9992–9997 (2013).
12. Gillmore, J. D. *et al.* Efficacy and safety of acoramidis in transthyretin amyloid cardiomyopathy. *N. Engl. J. Med.* **390**, 132–142 (2024).
13. Fontana, M. *et al.* Vutrisiran in patients with transthyretin amyloidosis with cardiomyopathy. *N. Engl. J. Med.* (2024) doi:10.1056/NEJMoa2409134.
14. Grogan, M. *et al.* Artificial intelligence-enhanced electrocardiogram for the early detection of cardiac amyloidosis. *Mayo Clin. Proc.* **96**, 2768–2778 (2021).
15. Goto, S. *et al.* Artificial intelligence-enabled fully automated detection of cardiac amyloidosis using electrocardiograms and echocardiograms. *Nat. Commun.* **12**, 2726 (2021).
16. Dorbala, S. *et al.* ASNC/AHA/ASE/EANM/HFSA/ISA/SCMR/SNMMI Expert Consensus Recommendations for Multimodality Imaging in Cardiac Amyloidosis: Part 1 of 2-Evidence Base and Standardized Methods of Imaging. *Circ. Cardiovasc. Imaging* **14**, e000029 (2021).
17. Sangha, V. *et al.* Detection of Left Ventricular Systolic Dysfunction From Electrocardiographic Images. *Circulation* (2023) doi:10.1161/CIRCULATIONAHA.122.062646.
18. Sangha, V. *et al.* Automated multilabel diagnosis on electrocardiographic images and signals. *Nat. Commun.* **13**, 1583 (2022).
19. Sangha, V. *et al.* Biometric contrastive learning for data-efficient deep learning from electrocardiographic images. *J. Am. Med. Inform. Assoc.* (2024) doi:10.1093/jamia/ocae002.

20. Mingxing Tan and Quoc V Le. EfficientNet: Rethinking model scaling for convolutional neural networks. *International Conference on Machine Learning, 2019*.
21. Selvaraju, R. R. *et al.* Grad-CAM: Visual Explanations from Deep Networks via Gradient-based Localization. *2017 Ieee International Conference on Computer Vision (Iccv)* 618–626 (2017).
22. Sun, X. & Xu, W. Fast implementation of DeLong's algorithm for comparing the areas under correlated receiver operating characteristic curves. *IEEE Signal Process. Lett.* **21**, 1389–1393 (2014).
23. DeLong, E. R., DeLong, D. M. & Clarke-Pearson, D. L. Comparing the areas under two or more correlated receiver operating characteristic curves: a nonparametric approach. *Biometrics* **44**, 837–845 (1988).
24. Alexander, K. M. *et al.* Geographic disparities in reported US amyloidosis mortality from 1979 to 2015: Potential underdetection of cardiac amyloidosis. *JAMA Cardiol.* **3**, 865–870 (2018).
25. Spencer-Bonilla, G. *et al.* Racial and ethnic disparities in transthyretin cardiac amyloidosis. *Curr. Cardiovasc. Risk Rep.* **15**, (2021).
26. Mora-Ayestaran, N. *et al.* Age- and sex-related differences in patients with wild-type transthyretin amyloidosis: Insights from THAOS. *JACC Adv.* **3**, 101086 (2024).
27. Martyn, T., Simkowski, J. M. & Hanna, M. Understanding race, genotype, and socioeconomic status in transthyretin amyloid cardiomyopathy: An area of deprivation. *JACC CardioOncol.* **6**, 464–466 (2024).
28. Shankar, B. *et al.* Race and socioeconomic status impact diagnosis and clinical outcomes in transthyretin cardiac amyloidosis. *JACC CardioOncol.* **6**, 454–463 (2024).

29. Maurer, M. S., Miller, E. J. & Ruberg, F. L. Addressing health disparities-the case for variant transthyretin cardiac amyloidosis grows stronger. *JAMA: the journal of the American Medical Association* vol. 331 1809–1811 (2024).

30. Falk, R. H. & Kattan, C. G. Black women and transthyretin amyloidosis: Insights from the women's health initiative. *JACC. Heart failure* vol. 11 1200–1202 (2023).

31. Martyn, T. *et al.* Racial and genetic differences in presentation of transthyretin amyloid cardiomyopathy with impaired left ventricular function. *JACC Heart Fail.* **10**, 689–691 (2022).

32. Patel, R. K. *et al.* Sex differences among patients with transthyretin amyloid cardiomyopathy - from diagnosis to prognosis. *Eur. J. Heart Fail.* **24**, 2355–2363 (2022).